PCCP

Boronated Holey Graphene: A case of 2D Ferromagnetic Metal

Journal:	*Physical Chemistry Chemical Physics*
Manuscript ID	CP-ART-05-2019-002936.R1
Article Type:	Paper
Date Submitted by the Author:	26-Aug-2019
Complete List of Authors:	Nafday, Dhani; Indian Association for the Cultivation of Science Fang, Hong; Virginia Commonwealth University Jena, Purusottam ; Virginia Commonwealth University Saha-Dasgupta, Tanusri; Satyendra Nath Bose National Centre for Basic Sciences

Journal Name

ARTICLE TYPE

Cite this: DOI: 00.0000/xxxxxxxxxx

Boronated Holey Graphene: A case of 2D Ferromagnetic Metal†

Dhani Nafday,[a], Hong Fang,[b] Puru Jena,[b] and Tanusri Saha-Dasgupta *[a,c]

Received Date
Accepted Date

DOI: 00.0000/xxxxxxxxxx

In search of new candidates for two-dimensional ferromagnets, we consider boronated monolayer holey graphene (C_2B), akin to recently synthesized and extensively studied nitrogenated monolayer holey graphene (C_2N). In contrast to C_2N which is semiconducting and nonmagnetic, our first-principles calculations show that C_2B is metallic and ferromagnetic. The microscopic origin of this interesting behavior is found to be related to the hole doping of $\pi - \pi^*$ network of C-B which produces metallicity while the unpaired electron on the dangling bond of sp^2 hybridized state of two-coordinated B produces magnetism. Calculated cohesive energy of boronated holey graphene indicates that the formation of this structure is energetically feasible as is the case with its nitrogenated counterpart. The dynamic and thermal stability of the predicted boronated holey graphene are checked in terms of phonon calculations and finite temperature molecular dynamics simulations. We further investigate the electronic and magnetic properties of embedded transition-metal single atom and pairs on C_2B and C_2N structures.

1 Introduction

The discovery of graphene and its wealth of exciting properties such as high carrier mobility,[1] gate-tunable charge concentration,[2] and anomalous quantum hall effect[3] have stimulated considerable interest in the study of atomically thin two-dimensional (2D) materials as well as quasi-2D materials of a few atomic-layers. Because of the potential applications of these materials, the field has subsequently expanded in terms of synthesis of graphene-based derivatives with a goal to further improve their properties. In this connection, holey graphene,[4] which consists of a periodic array of nanosized holes within the backbone of graphene, has attracted a great deal of attention. The presence of holes leads to the formation of one-dimensional channels which enables holey graphene with good semiconducting properties.[5] In addition, the dependence of the band gap on the size of the nanohole[5] makes it a suitable candidate for band gap engineering. Continuing in this direction, in 2015, a new 2D holey-graphene derivative known as nitrogenated holey graphene was successfully synthesized.[6] This material has a C_2N stoichiometry and consists of a 2D sheet formed by periodic arrangement of pair of benzene rings bridged by a pyrazine ring. It is found to be nonmagnetic and a direct band gap semiconductor with a band gap of 1.96 eV.[6] C_2N based field effect transistors have already been demonstrated to show a good ON/OFF ratio of 107.[7] Possible applications of this material in opto-electronic devices and photocatalysis[8] have further fuelled interest in doped holey graphene.

While all the above-mentioned progress is remarkable in its own right, what is missing is the intrinsic magnetic order in a single 2D carbon based layer. The importance of this topic is highlighted in the title of the Editorial in Nature Nanotechnology,[9] "2D magnetism gets hot". The 2D magnetism can appear in localized spin system through inclusion of magnetic anisotropy in a Heisenberg model as found in case of $Cr_2Ge_2Te_6$[10] or CrI_3[11]. It can also appear in metallic layered material due to enhanced density of states at the Fermi level leading to magnetic order governed by the Stoner criterion.[12] Recently,[13] ferromagnetic (FM) order in monolayers of VSe_2 grown on either graphite or $MoSe_2$ substrate has been demonstrated which has been suggested due to enhanced density of states at the Fermi level. Following these exciting developments, there is a surge of activity to find other candidate materials exhibiting 2D ferromagnetism. In this context, metal-free *p*-electron based ferromagnets form attractive choices as they are expected to have a long spin relaxation time owing to the presence of weak spin-orbit coupling.[14–16] Along this idea, edge magnetism in graphene has been discussed,[17] whose usefulness and applicability still remains to be established on a firm ground. Ab-initio studies[18,19] considering carrier doping via additional C atoms or gating of nitrogenated holey graphene have predicted metallic ferromagnetism. Other than ni-

[a]*School of Mathematical and Computational Sciences, Indian Association for the Cultivation of Science, Kolkata 700 032.*
[b]*Department of Physics, Virginia Commonwealth University, Richmond, Virginia 23284, USA.*
[c]*Department of Condensed Matter Physics and Materials Science, S. N. Bose National Centre for Basic Sciences, Kolkata 700098, India. Fax: +91-33-2335-3477; Tel: +91-33-2335-5707; E-mail:t.sahadasgupta@gmail.com*

trogenation, alloying of holey graphene with other elements has not been reported, although theoretical study has been carried out for phosphorated and arsenicated holey graphenes.[20] Calculated cohesive energy indicated that, similar to the C_2N monolayer, formation of phosphorated and arsenicated holey structures are also energetically feasible, making the situation promising.

Motivated by these findings, we consider in the present study boronated holey graphene. Substitution of carbon by boron, has been demonstrated to be an extremely useful route to introduce flexibility in 2D MXene structure[21,22] and in the manipulation of Stone-Wales defect in fullerene.[23] It is to be noted that nitrogenation, phosphoration, or arsenication of holey graphene leads to electron doping, while boronation leads to hole doping. Pairing of p_z electrons of C atoms and N/P/As atoms, with the lone pair being located on the dangling bond of two-coordinated N/P/As sites in the nitrogenated, phosphorated or arsenicated structures leads to nonmagnetic and semiconducting ground state.[6,24] On the other hand, introduction of B atoms in the two-coordinated positions of the holey structure having one electron less than that of C atoms, increases the possibility of magnetism as well as metallicity. This may cause stabilization of 2D magnetism in a metallic system through Stoner criterion.[12] In the following, we explore this possibility in C_2B through first-principles calculations, and compare the results to that of C_2N. We also explore the properties of boronated holey graphene structure by embedding single and pairs of 3d transition metal (TM) atoms such as Sc and Mn in the nano-holes.

2 Computational Details

The first principle calculations are carried out within the framework of density functional theory (DFT) based on projector augmented wave (PAW) pseudopotentials as implemented within the Vienna *Ab-Initio* Simulation Package.[25] The wave functions are expanded within the plane-wave basis set with a kinetic energy cut-off of 500 eV. Full geometry relaxations, involving both volume and atomic coordinates, are performed within the generalized gradient approximation (GGA) as parametrized by Perdew-Burke-Ernzerhof (PBE).[26] Possible Van-der-Waals interactions, which may be important for 2D materials, are included within DFT-D2 approach.[27] The structures are relaxed towards equilibrium until the Hellmann-Feynman forces becomes less than 0.0001 eV/Å^3. A Γ-centered k-mesh of 32 × 32 × 1 is used for the unit cell calculations.

The dynamical and thermal stability of C_2B structure are verified using phonon calculations and molecular dynamics (MD) simulation at 300 K, respectively. Phonons are calculated using density functional perturbation theory (DFPT). Molecular dynamic simulations are conducted using the *NVT* ensemble, where the shape of the cell is allowed to change. A time step of 1 fs is used. The simulation lasts for a total of 7 ps, with the first 2 ps for the system to reach thermal equilibrium.

For the calculations of transition metal(s) in embedded structures, supercells of size 2 × 2 × 1 for single TM atom and 3 × 2 × 1 for TM atom pair are used and calculations are carried out using 8 × 8 × 1 k-mesh. A Gaussian smearing with smearing value of 0.005 eV is used for the Brillouin Zone integration. In order to take into account the strong correlation effect beyond GGA, a supplemented on-site Coulomb interaction, U of 4 eV is applied at the TM sites within the GGA+U framework.[28] In order to estimate the correct site preference of the TM atoms embedded in the hole, the TM atoms are initially placed at the centre of the hole and subsequently kicked off-centre in five incremental steps along the *b* and *a* directions of the hexagonal lattice.

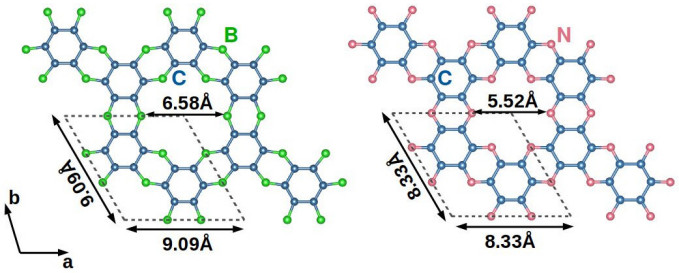

Fig. 1 Optimized crystal structure of C_2B (left panel) and C_2N (right panel), viewed along the hexagonal *c*-axis. Marked are the diameters of the holes in the structures, the lattice constants of the 2D hexagonal lattices, and the unit cells with dashed lines.

3 Results and Discussion

3.1 Properties of C_2B

We start our discussion by considering the structural, electronic and magnetic properties of C_2B in comparison to that of the well studied case of C_2N. This discussion brings out the contrast between hole doping and electron doping at the two-coordinated sites of holey graphene.

3.1.1 Structure and the Stability.

The optimized structure of monolayer C_2B compared to that of C_2N is shown in Fig. 1. The computed structure of C_2N is found to be in good agreement with that reported previously[29] First of all, the lattice constant is found to be expanded by about 9% upon replacement of N by B, with C-B bondlength more than 10% longer than C-N bondlength (see Table I). Furthermore the B-containing ring connecting two benzene rings in C_2B is squeezed, as opposed to the N-containing ring connecting two benzene rings in C_2N which is elongated. This is due to the fact the C-B (N) bond is longer (shorter) than C-C bond(s) in the boronated (nitrogenated) holey structure. Together, these cause the radius of the hole in C_2B to expand substantially (by about 19%) compared to that in C_2N. The distortion of the benzene ring is found to be similar between the two structures.

Table 1 Various bondlengths of the theoretically calculated C_2B and C_2N monolayers

Bondlength(Å)	C_2B	C_2N
C-C(along hexagonal *b* axis)	1.422	1.429
C-C(along hexagonal *a* axis)	1.466	1.469
C-N(B)	1.475	1.336

The calculated cohesive energy of the optimized C_2B structure turns out to be 6.61 eV, compared to 7.54 eV for C_2N. This

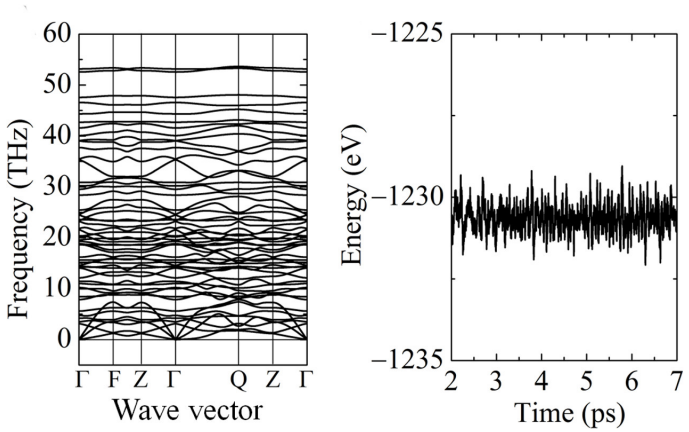

Fig. 2 Left: Calculated phonon spectrum for C_2B showing no imaginary frequencies indicating the structure is lattice dynamically stable. Right: Molecular dynamics simulation at room temperature on the structure for 5 ps, showing good thermal stability.

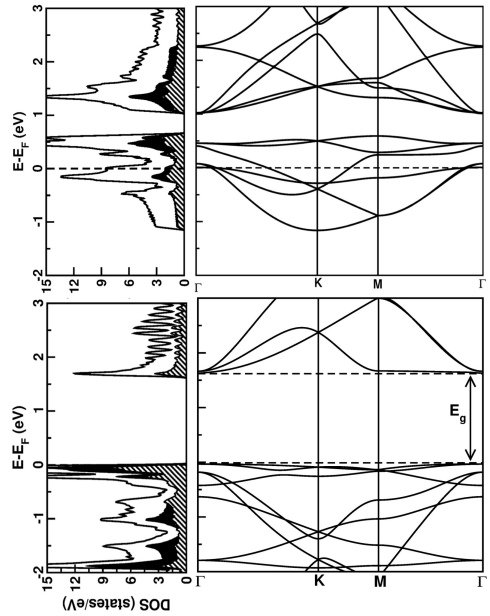

Fig. 3 The calculated non spin-polarized density of states (left) and band structure (right) of C_2B (top panels) and C_2N (bottom panels). The zero of the energy is set at Fermi energy, E_F. In the density of states plots, shown are the total density of states (solid line), and that projected to B/N states (shaded) and C states (hatched). The direct band-gap of C_2N is marked.

strongly indicates that formation of C_2B structure is feasible like C_2N. We note that the cohesive energy of proposed C_2B structure is smaller than that of C_2N, while it is comparable to that of C_2P.[20] The formation energy for the boronated holey graphene, defined as,[30]

$$\Delta E = \frac{1}{m_B}\left[E_t(BG) - E_t(PG) - m_B\mu_B + m_B\mu_C\right] \quad (1)$$

is further calculated, and compared to that of B-doped graphene and B-doped diamond alloy, where $E_t(BG)$ and $E_t(PG)$ are the total energies of holey graphene/graphene/diamond with and without doped B atom and m_B is the number of doped B atoms. μ_B and μ_C are the chemical potentials of the boron atom and carbon atom respectively, which are taken as total energies per atom of α-boron crystal and pristine holey graphene/graphene/diamond. The calculation show the stability of boronated holey graphene to be comparable to B-doped diamond (0.86 eV for B-doped holey graphene and 0.91 eV for B-doped diamond) while the formation energy of B-doped graphene is found to be 1.87 eV.

Monolayer C_2B is found to be lattice dynamically stable as shown by the calculated phonon spectrum in left panel of Fig. 2, where no imaginary frequencies are found. Molecular dynamics simulations at room temperature (300 K) also show good thermal stability of the structure at room temperature (Fig. 2, right panel). The in-plane stiffness constant C, for the stable C_2B monolayer structure, calculated from the slope of the linear region of the stress-strain curve is found to be 269.9 GPa, compared to the value of 340.8 GPa estimated for pristine graphene.[31,32] The in-plane stiffness of C_2B, is thus found to be somewhat less than that of graphene, though of same order, suggesting more flexibility of 2D boronated holey graphene structure, compared to that of graphene.

3.1.2 Electronic Structure and Magnetism.

Since the possible magnetism of C_2B is expected to originate from instability in a metallic system, we first examine the non-magnetic electronic structure of C_2B, to check the instability of the non-magnetic solution. For comparison, we also present the results for C_2N which is known to be non-magnetic and semiconducting.

The electronic structure of C_2B, namely the band structure and the density of states (DOS) calculated within the non spin-polarized scheme of calculation, is shown in Fig. 3 and compared to that of C_2N. In agreement with previous literature,[29] it is noted that C_2N is a direct band-gap semiconductor as both the valence band maxima (VBM) and conduction band minima (CBM) lie at the Γ-point. Our estimated value of 1.64 eV for the band gap agrees well with previously reported theoretical values[29] but is smaller than the experimental gap of 1.96 eV.[6] Such a discrepancy between the experimental and theoretical value is expected due underestimation of the DFT band gap. The VBM dominated by N states, arises due to the formation of flat bands contributed by highly localized lone pair in sp^2 hybridized σ orbital. As pointed out previously, this remains non-bonded at the two-coordinated N site.[6,24] The CBM, on the other hand, is contributed by dispersive π^* orbital of C, delocalized over plane, together with flat band originating from localized π^* state at N atom site.

Interestingly, in contrast to pristine C_2N, the electronic structure calculation of C_2B yields metallic solution. This arises due to the fact that the out-of-plane π (p_z) orbital of the B atom is empty as opposed to being singly occupied as in the case of C or N. This leads to hole-doping of the delocalized π-π^* bond network of C_2B resulting in the shifting down of the Fermi level below the valence band. Consequently, the system becomes metallic in character. The presence of substantial density of states at the Fermi energy (E_F) is noted in non spin-polarized DOS of C_2B, with a value of 8.49 states/eV. This suggests the instability of the non-

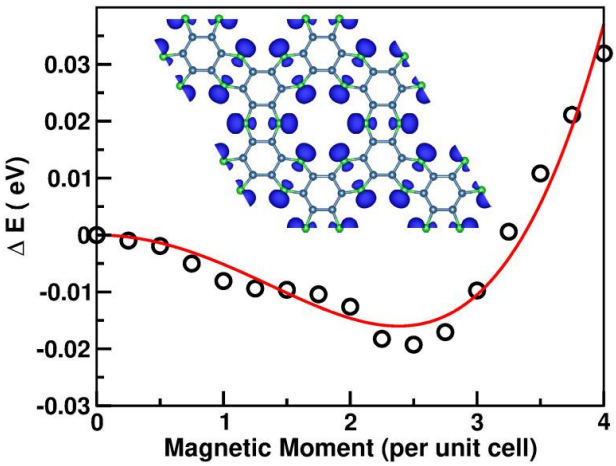

Fig. 4 Calculated total energy of C_2B, plotted as a function of constrained values of the magnetic moment in the unit cell. The solid line is the fit to the calculated data points. The inset shows the plot of the magnetization density with a chosen isovalue of 0.005 $e^-/Å^3$.

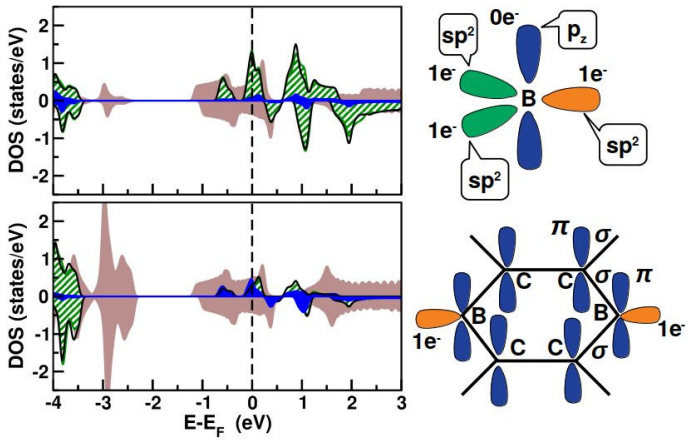

Fig. 5 Spin polarized density of states of C_2B, projected to B (top panel) and C (bottom panel) s (shaded blue), p_x(hatched green), p_y(black) and p_z(brown) states. The zero of energy is fixed at E_F. Shown by the side are the schematics of the nature of bonding and occupancies of B atom in the C_2B network. Two out of three electrons of B occupy the sp^2 hybridized σ bonded state with in plane C atoms (marked in green), the remaining electron occupy the sp^2 hybridized dangling bond (marked in yellow), and the out-of-plane p_z orbital (marked in blue) forming π bonding with C atoms remains empty.

magnetic solution towards a stable magnetic solution following Stoner's criteria [12,33] of band magnetism.

In order to ascertain the magnetic properties of C_2B, fixed moment calculations are carried out constraining the total moment in the cell to fixed values. This gives rise to estimates of total energy as a function of magnetic moment, as presented in Fig. 4. The calculated data points are fitted to the curve given by the polynomial equation

$$E = E_0 + a_2M^2 + a_4M^4 \quad (2)$$

where E is the energy for a given magnetic moment M, E_0 is the energy of the non-magnetic solution and a_2, a_4 are the fitting parameters. The value of a_2 is directly related to the Stoner parameter I_s by the formula $a_2 = \frac{1}{N(E_F)} - I_s$ where $N(E_F)$ is the density of states at E_F. Using the estimates of a_2 as obtained from the fitting and the $N(E_F)$ value read from the non spin polarized DOS, the calculated value of $I_sN(E_F)$ turns out to be 1.2 which satisfies the Stoner criteria for a magnetic solution.

The spin-polarized calculation gives rise to a total magnetic moment of 2.49 μ_B/unit-cell, the minimum in E versus M curve. The inset in Fig. 4 shows the plot of the magnetization density, which shows that the magnetization is primarily contributed by B atoms. This is corroborated by the calculated magnetic moment of ≈ 0.16 μ_B at B site and a tiny moment of 0.01 μ_B at C site. The spin-polarized DOS projected onto B/C s, p_x/p_y and p_z states is presented in Fig. 5, which shows a large contribution of B p_x/p_y, together with B s states in producing the spin-splitting, while B p_z admixed with C p_z gives rise to metallicity. The microscopic understanding of this curious metallic magnetism is schematically shown by the side of Fig. 5. As shown in the top schematic panel, similar to carbon and nitrogen, the boron atom, having electron configuration [He]$2s^22p^1$, also undergoes sp^2 hybridization. However, since boron has one and two electrons less compared to carbon and nitrogen, respectively, the out-of-plane p_z orbital becomes empty. Consequently the p_z orbital of B becomes empty, and the dangling bond is occupied by one electron instead of two, as in case of N in C_2N. This results in hole doping of the $\pi - \pi^*$ bonded network of C and B in C_2B, giving rise to metallicity, as mentioned above. Furthermore, the unpaired electron occupying the non-bonded sp^2 (marked in yellow in the Fig. 5) within the two coordinated geometry of B in C_2B being localized, gives rise to magnetism. Antiferromagnetic configuration is found to be less favorable than the ferromagnetic configuration.

3.2 Effect of embedding *3d* TM atom

As suggested in previous studies,[24] embedding of 3d TM atoms in holey graphene systems can significantly affect their properties. Depending on the choice of the embedded TM atom and its site preference, metallic, semi-metallic and semiconducting behaviors have been reported.[34] In the following, we discuss the effect of embedding Sc and Mn, representatives of early and late 3d TM atoms, respectively. Calculated work functions for Sc and Mn coverage on C_2B and C_2N result in values 4.39 eV for Sc-C_2N, 4.45 eV for Sc-C_2B, 4.37 eV for Mn-C_2N and 4.47 for Mn-C_2B.

Note that bulk Sc is nonmagnetic while bulk Mn is antiferromagnetic. In addition, Mn with an electronic configuration of $3d^54s^2$ has a magnetic moment of 5 μ_B. Our objective is to see if these transition metal atoms retain their atomic magnetic moment upon embedding? If so, how do they couple to an adjacent transition metal atom.

3.2.1 Single TM

We study TM embedding in boronated (nitrogenated) holey graphene structures by considering $2 \times 2 \times 1$ supercells of C_2B (N), and positioning the TM atom in the central hole of the cell. This makes the periodic images of TM atoms separated by distance of 17-18Å, which minimizes their interactions, mimicking the isolated limit.

The first step is to find the preferred site of TM inside the hole,

Table 2 The off-centering (δ) of the TM atom within the hole, the binding energy (BE) of TM embedding, the C-X (X= N,B) bondlength for the X atom facing the TM atom (b_{C-X}), the magnetic moments at the TM site, N/B site and the total moment in the 2 × 2 × 1 cell. The last column shows the spin-polarization, $P(\%)$, of the TM embedded systems.

System	δ (Å)	BE (eV)	b_{C-X} (Å)	Mag. Mom. (μ_B)			P (%)
				TM	N/B	Cell	
Sc-C_2N	0.26	7.04	1.393	0.72	0.02-0.05	1.92	50.1
Mn-C_2N	0.59	4.08	1.375	4.75	-0.04-0.05	4.99	94.9
Sc-C_2B	0.00	8.24	1.559	0.62	0.01-0.11	5.74	24.7
Mn-C_2B	0.00	5.12	1.532	4.64	0.04-0.09	7.13	16.9

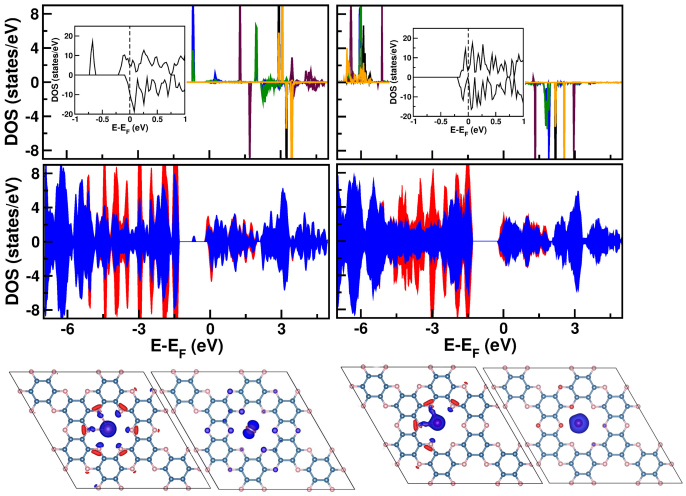

Fig. 6 The spin-polarized density of states (top and middle panels) and the charge density differences along with magnetization density (bottom panels) of Sc (left panels) and Mn (right panels) embedded C_2N. The top panels show the DOS projected on to TM d states, with d states of $d_{x^2-y^2}$, $d_{3z^2-r^2}$, d_{xy}, d_{xz}, d_{yz} symmetries colored as yellow, magenta, black, green and blue, respectively. Insets in top panels show the zoomed plot to total DOS close to E_F. The middle panels show the DOS projected to C (blue) and B (red) states. The zero of the energy is set at E_F. The bottom panels show the plot of charge density difference plotted at isovalue 0.03 e^-/Å^3 (blue represents positive charge density difference(left panel) and red represents negative charge density difference), and the magnetization density (right panel, with isovalue 0.005 e^-/Å^3) of the systems.

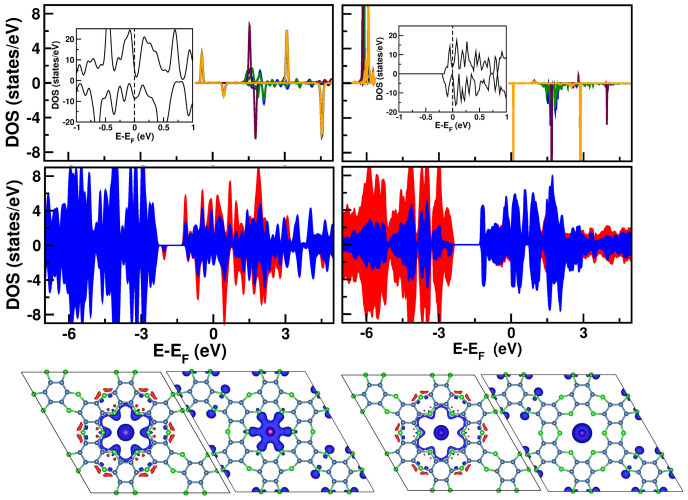

Fig. 7 Same as Figure 6, but shown for TM(s) embedded in C_2B.

since the properties are influenced by its position. For example, semiconducting behavior is reported when Sc atom is positioned at the center of the hole in pristine C_2N while metallic behavior is reported when the Sc atom is embedded in C_2N at an off-centered position.[34] Apart from the central site in the hole, two other possible sites exist. These are, between the central site of the hole and the bridge site of the benzene ring, and that site between the central site and the hollow site of the C-B/N ring.[34] Our detailed calculation shows that Sc prefers to occupy the central site of the hole for C_2B, while it prefers to occupy the off centered site lying between the central site and the bridge site of the carbon ring (See Fig. 6 and 7, and Table II) in case of C_2N.[35]

This is at first surprising because the hole size in C_2B is substantially larger compared to C_2N. This is attributed to the fact that the electron cloud of B atoms around the edge of the hole in C_2B is more delocalized than that of N in C_2N, as evident from the plots of the magnetization density and the charge density difference in C_2B/C_2N with and without embedded atom (see bottom panels in Fig. 6 and 7). This effectively reduces the size of the hole, thus preventing Sc atom to occupy an off-centered position due to $e^- - e^-$ repulsion.

On the other hand, in the case of semiconducting C_2N with localized states, the size of Sc atom (covalent radius = 1.84 Å) is much smaller than size of the hole (5.52 Å), which results in the Sc atom preferring to occupy an off-centered position. This allows formation of asymmetric covalent bonding with some of the N atoms at the edge of the hole, as seen in the magnetization density plots presented in bottom panels of Fig. 6. Very similar trend is observed for embedding of Mn atom (see Table II). It is interesting to note, that the embedding energy, defined as $E_b = E_{TM} + E_{C_2B/N} - E_{TM-C_2B/N}$, where E_{TM}, $E_{C_2B/N}$, $E_{TM-C_2B/N}$ are the energies of the isolated metal atom in the same volume, C_2B/C_2N and metal embedded-C_2B/C_2N, receptively, is substantially high for C_2B compared to C_2N, driven by stronger covalency between TM atom and relatively delocalized unpaired electron of B, compared to localized lone pair of N. The binding energies for Sc embedded in C_2B turned to be 17% larger than that of C_2N, while it is about 26% larger than that of C_2N for Mn embedding. This in turn causes significant change in the TM-embedded C_2B network with stretching of C-B bonds, as shown in Table II.

The top and middle panels of Fig. 6 and Fig. 7, show the spin-polarized density of states of Sc-embedded C_2N and C_2B (left panels) and Mn-embedded C_2N and C_2B (right panels), respec-

tively. The states are projected to TM d states (top panels) and C and N/B states (middle panels). Within the Sc-C_2N/B network, the Sc d states are hybridized with the N or B sp^2 states, the hybridization being much stronger for B with unpaired electron at dangling bond, compared to that for N with localized lone-paired electron. Due to higher electro-negativity of the nitrogen/boron atoms, charge is transferred from the Sc atom to the C_2N or C_2B sheet. This is supported by the fact, that the local moment on Sc is reduced to 0.72 (for C_2N) or 0.62 μ_B (for C_2B), compared to fully localized estimate of 1.0 μ_B (see Table II). The crystal field splitting introduced at the TM sites by the six surrounding B atoms splits the TM sites d states, making the $d_{x^2-y^2}/d_{xy}$ the lowest in energy, followed by $d_{3z^2-r^2}$ and others. In the case of TM embedding in C_2B, bonding $d_{x^2-y^2}/d_{xy}$ state of Sc atom becomes occupied in majority spin channel, keeping other d states empty. All the d states of Mn gets occupied in majority spin channel and remains empty in minority spin channel, in accordance with d^5 occupancy of Mn. In contrast, the off-centering of Sc and Mn atoms, makes the crystal field splitting of d states at TM site different in case of C_2N (see Fig. 7).

The net moment in the cell for Sc and Mn embedded C_2B is largely enhanced compared to C_2N due to additional magnetic contribution of B atoms. It is interesting to note incorporation of external atom in the network causes distribution of magnetic moments at N or B sites. For TM embedded in C_2N this primarily happens due to off-centred position of TM atoms, which naturally lowers the symmetry. For C_2B system this also happens, even though the TM sites occupy the central position in the hole. As is evident from the magnetization density plots (cf Fig. 7), upon incorporation of the TM atom, the magnetic moment at B sites in the vicinity of TM atom decreases substantially compared to that at B sites far away from TM site. In fact, the moment at B sites in the vicinity of the embedded atom vanishes completely in case of Mn.

The plots of total DOS (see insets in Fig. 6 and 7) suggest high degree of spin polarization of the carriers in certain cases. We thus compute the degree of spin-polarization, defined as $P = \frac{N_\uparrow - N_\downarrow}{N_\uparrow + N_\downarrow}$, where $N_\uparrow$ and $N_\downarrow$ represent DOS at E_F in the majority and minority spin channels, respectively. The results are listed in the last column of Table II. The degree of spin-polarization in general is found to be higher for C_2N compared to C_2B, which once again demonstrates that the delocalized character of C_2B interacting with TM atoms is stronger than that in C_2N. As is seen, the system is found to be at the verge of being half-metallic for Mn-C_2N, indicating the possible application of Mn embedded C_2N monolayers in spintronics application.

We thus conclude that while embedding of TM atoms in boronated holey graphene is effective for producing 2D magnets with large moment, the degree of carrier spin-polarization achieved is generally larger for C_2N.

3.2.2 TM pair

We next consider placing two TM atoms in two neighboring holes along hexagonal a-direction within a 3 × 2 × 1 cell. This results in intra-pair separation of around 7.5Å separated by distance of 17-18Å from their periodic images. This is in contrast to the calculations carried out in Ref.20 where a supercell of 2 × 2 × 1 was used, thereby making a chain of TM atoms running along the hexagonal a-direction. Considering two TM embedded configurations, we compute the energies for the FM, and antiferromagnetic (AFM) alignment of TM spins. The difference of the total energies in two cases ($E_{AFM} - E_{FM}$) is defined as the exchange energy (E_{ex}). Table III lists the exchange energies of Sc$_2$-C_2N, Mn$_2$-C_2N, Sc$_2$-C_2B and Mn$_2$-C_2B. Ferromagnetic coupling is preferred in all cases, as evidenced from positive values of E_{ex}'s. This is in accordance with the results reported earlier[24] for C_2N, although the configuration considered was a chain configuration, as mentioned above. We find our computed exchange energies for C_2N systems to be significantly smaller than that reported in Ref.20 which evidently stems from the consideration of two different systems (isolated pair versus chain) in two studies. This is in line with the ferromagnetic characters of atomic chains of TM atoms from Sc to Co, absorbed on monolayer MX (M = Si/Ge, X = P/As).[36] We further notice that the exchange energies in case of TM pairs embedded in C_2B are much smaller compared to that in C_2N, justified by the fact that due to off-centring of TM atoms within the hole of C_2N, the intra-pair distance of TM atoms in C_2N is much smaller compared to that in C_2B (7.6 Å in C_2N versus 8.7 Å in C_2B).

Table 3 The exchange energies (E_{ex}) for Sc- and Mn-pairs embedded in 3 × 2 × 1 cell of C_2N and C_2B. Magnetic moments refer to the total moment in the 3 × 2 × 1 cell.

Systems	E_{ex} (meV)	Mag. Mom (μ_B)
Sc$_2$-C_2N	9.31	2.04
Mn$_2$-C_2N	17.62	8.00
Sc$_2$-C_2B	2.13	15.78
Mn$_2$-C_2B	2.06	22.77

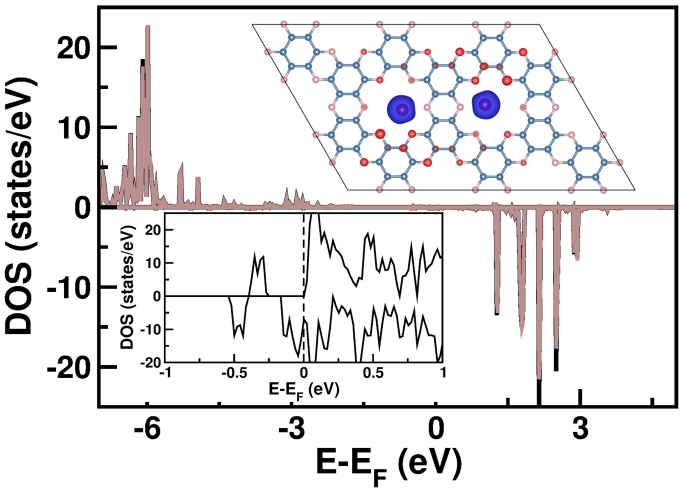

Fig. 8 The spin-polarized density of states projected to Mn d states in Mn$_2$-C_2N system. The insets magnetization density (top) with blue and red colors signifying up and down spin densities, and the plot of total density of states zoomed at E_F (bottom).

The ferromagnetic exchange between pair of Mn atoms em-

bedded in C_2B or C_2N is interesting and needs separate mention. The half-filled 3d shell of Mn, according to Hund's rule, gives an atomic magnetic moment of 5 μ_B. Introduction of ferromagnetic coupling between Mn atoms is thus expected to produce a large net moment, which is of technological importance. The magnetic moments of Mn_2 embedded in a rare gas matrix, however, are coupled antiferromagnetically.[37] In medium to large sized Mn clusters containing 11 to 100 atoms, the magnetic coupling is ferrimagnetic, with net magnetic moments less than 1.5 μ_B/atom. On the other hand ferromagnetic coupling of Mn_5 cluster isolated in rare gas matrix and carrying a total moment of 25μ_B has been observed in electron spin resonance.[38] A giant magnetic moment of 22 μ_B has also been theoretically predicted for nitrogen-doped Mn_5 cluster.[39]

Our predicted ferromagnetic exchange between pair of Mn atoms embedded in nitrogenated or boronated holey graphene would be another possible means to achieve large moment by ferromagnetic alignment of spins. Indeed, our calculations revealed ferromagnetic coupling between Mn pair embedded in C_2B produces a giant moment of 22.8 μ_B in the $3 \times 2 \times 1$ cell. Considering a $3 \times 2 \times 1$ supercell of pristine boronated holey graphene, a magnetic moment of 14.94 μ_B (6×2.49 μ_B) is obtained which gets further enhanced to 22.8 μ_B due to parallel alignment of embedded Mn pairs in the high spin state.

Interestingly, pair of Mn atoms embedded in C_2N are not only ferromagnetically coupled, with the scale of ferromagnetic exchange being about 200 K, but also possess an integer net moment. Mn atoms contribute a moment of 9.2 μ_B, with 4.6 μ_B moment on each Mn, while the moments at N atoms in the vicinity of Mn atoms aligning antiparallel to that of Mn spins (cf. Fig. 8), contribute -1.2 μ_B, making a net magnetic moment of 8 μ_B in the cell. The total DOS of the system shows half-metallic behavior, as shown in Fig. 8. This interesting situation calls for further investigation.

4 Conclusions

In summary, inspired by recent success in the synthesis of nitrogenated holey graphene,[6] we explore the effect of boronation at the two coordinated site of monolayered holey graphene. Introduction of B in place of N, introduces drastic change in the properties of these monolayers. Calculations of total energies show that the proposed boronated compound is stable. The dynamical and thermal stability of this compound is also established from calculations of phonon band structure and ab initio molecular dynamics at 300 K. Thus, it should be possible to synthesize boronated holey graphene.

Based on our first-principles calculations, we propose that boronated holey graphene is a candidate material for 2D ferromagnetism. This is in marked contrast with properties of C_2N, which is nonmagnetic and semiconducting. The origin of this metallic 2D magnetism is traced to hole doping of $\pi - \pi^*$ network of C-B together with creation of unpaired electron in the sp^2 hybridized orbital on the dangling bond of B. Encouraged by the observation of 2D metallic ferromagnetism in pristine C_2B, we study embedding of transition metal atoms in the holes of the boronated holey graphene. We use Sc, as an example of early transition metal, and Mn, as an example of late transition metal. We consider embedding of both isolated atom and atom pairs at two neighboring holes.

In contrast to the situation with C_2N, we find embedded atoms occupy the central site inside the hole in C_2B, driven by the electrostatic repulsion from the unpaired electron at the dangling bond of the B site. The metal atom-embedded boronated systems show large magnetic moments, contributed by both the metal atom(s) and the boron atoms, while the metal atom-embedded nitrogenated systems show larger degree of spin-polarization, being at verge of being half-metallic when Mn is embedded. The exchange interaction between metal pairs turned out to ferromagnetic both for C_2N and C_2B, with gigantic net moment for Mn_2-C_2B, and half-metallic ferromagnetism with large exchange for Mn_2-C_2N.

Conflicts of interest

There are no conflicts to declare.

Acknowledgements

TS-D thanks the Department of Science and Technology, India for the support through Thematic Unit of Excellence. P. J. acknowledges support of the U.S DOE, Office of Basic Energy Sciences, Division of Material Sciences and Engineering under Award No. DE-FG02-96ER45579.

Notes and references

1 A. Geim and K. Novoselov, *Nature Materials*, 2007, **6**, 183.
2 K. Kechedzhi, E. Hwang and S. D. Sarma, *Physical Review B*, 2012, **86**, 165442.
3 P. Ostrovsky, I. Gornyi and A. Mirlin, *Physical Review B*, 2008, **77**, 195430.
4 Y. Lin, Y. Liao, Z. Chen and J. W. Connell, *Materials Research Letters*, 2017, **5**, 209.
5 C. Moreno, M. Vilas-Varela, B. Kretz, A. Garcia-Lekue, M. V. Costache, M. Paradinas, M. Panighel, G. Ceballos, S. O. Valenzuela, D. Peña *et al.*, *Science*, 2018, **360**, 199.
6 J. Mahmood, E. K. Lee, M. Jung, D. Shin, I.-Y. Jeon, S.-M. Jung, H.-J. Choi, J.-M. Seo, S.-Y. Bae, S.-D. Sohn *et al.*, *Nature communications*, 2015, **6**, 6486.
7 T. Zhang and L. Zhu, *Physical Chemistry Chemical Physics*, 2017, **19**, 1757.
8 X. Luo, G. Wang, Y. Huang, B. Wang, H. Yuan and H. Chen, *Physical Chemistry Chemical Physics*, 2017, **19**, 28216.
9 Editorial, *Nature Nanotechnology*, 2018, **13**, 269.
10 C. Gong, L. Li, Z. Li, H. Ji, A. Stern, Y. Xia, T. Cao, W. Bao, C. Wang, Y. Wang *et al.*, *Nature*, 2017, **546**, 265.
11 B. Huang, G. Clark, E. Navarro-Moratalla, D. R. Klein, R. Cheng, K. L. Seyler, D. Zhong, E. Schmidgall, M. A. McGuire, D. H. Cobden *et al.*, *Nature*, 2017, **546**, 270.
12 E. C. Stoner, *Proceedings of the Royal Society of London. Series A. Mathematical and Physical Sciences*, 1938, **165**, 372.
13 M. Bonilla, S. Kolekar, Y. Ma, H. C. Diaz, V. Kalappattil, R. Das, T. Eggers, H. R. Gutierrez, M.-H. Phan and M. Batzill, *Nature nanotechnology*, 2018, **13**, 289.

14 W. Han, R. K. Kawakami, M. Gmitra and J. Fabian, *Nature nanotechnology*, 2014, **9**, 794.

15 G. Z. Magda, X. Jin, I. Hagymási, P. Vancsó, Z. Osváth, P. Nemes-Incze, C. Hwang, L. P. Biro and L. Tapaszto, *Nature*, 2014, **514**, 608.

16 J. Zhou, Q. Wang, Q. Sun, X. Chen, Y. Kawazoe and P. Jena, *Nano letters*, 2009, **9**, 3867.

17 T. Enoki and Y. Kobayashi, *Journal of Materials Chemistry*, 2005, **15**, 3999.

18 I. Choudhuri and B. Pathak, *ChemPhysChem*, 2017, **18**, 2336.

19 J. Zhu, Y. Zhao, S. Zeng and J. Ni, *Physics Letters A*, 2017, **381**, 1097.

20 M. Yagmurcukardes, S. Horzum, E. Torun, F. M. Peeters and R. T. Senger, *Physical Chemistry Chemical Physics*, 2016, **18**, 3144.

21 P. Chakraborty, A. Chakrabarty, A. Dutta and T. Saha-Dasgupta, *Physical Review Materials*, 2018, **2**, 103605.

22 P. Chakraborty, T. Das, D. Nafday, L. Boeri and T. Saha-Dasgupta, *Physical Review B*, 2017, **95**, 184106.

23 M. Kabir, S. Mukherjee and T. Saha-Dasgupta, *Physical Review B*, 2011, **84**, 205404.

24 J. Du, C. Xia, W. Xiong, X. Zhao, T. Wang and Y. Jia, *Physical Chemistry Chemical Physics*, 2016, **18**, 22678.

25 G. Kresse and J. Furthmüller, *Physical review B*, 1996, **54**, 11169.

26 J. P. Perdew, K. Burke and M. Ernzerhof, *Physical review letters*, 1996, **77**, 3865.

27 S. Grimme, *Journal of computational chemistry*, 2006, **27**, 1787.

28 S. Dudarev, G. Botton, S. Savrasov, C. Humphreys and A. Sutton, *Physical Review B*, 1998, **57**, 1505.

29 R. Zhang, B. Li and J. Yang, *Nanoscale*, 2015, **7**, 14062.

30 T. M. Dieb, Z. Hou and K. Tsuda, *The Journal of chemical physics*, 2018, **148**, 241716.

31 Q. Peng, C. Liang, W. Ji and S. De, *Physical Chemistry Chemical Physics*, 2013, **15**, 2003.

32 Q. Peng and S. De, *Physical Chemistry Chemical Physics*, 2013, **15**, 19427.

33 S. Blundell, *Magnetism In Condensed Matter*, Oxford University Press, Inc, New York, 1st edn, 2001.

34 D. Ma, Q. Wang, X. Yan, X. Zhang, C. He, D. Zhou, Y. Tang, Z. Lu and Z. Yang, *Carbon*, 2016, **105**, 463.

35 Note that our estimate of off-centering in case of C_2N turned out to be different from that reported in Ref.20.

36 S. Li, M. Zhou, F. Zheng and P. Zhang, *Advanced Electronic Materials*, 2019, **5**, 1800450.

37 M. D. Morse, *Chemical Reviews*, 1986, **86**, 1049.

38 C. Baumann, R. Van Zee, S. Bhat and W. Weltner Jr, *The Journal of Chemical Physics*, 1983, **78**, 190.

39 B. Rao and P. Jena, *Physical review letters*, 2002, **89**, 185504.